ARTICLE | Article in Press

Erosive wear behaviour of polymer matrix composites reinforced with temperature varied biochar using experimental and machine learning approaches

Smitirupa Pradhan · Prajapati Naik · Rakesh Kumar Tota · Kamesh Bodduru · Nankwaya Ntumba Zacharie

Received: 21 May 2026 / Accepted: 26 October 2026
© The Author(s) 2026

Abstract

This study investigates the application of machine learning (ML) techniques to analyze and predict the influence of carbonization temperature on the erosive wear behaviour of biochar-reinforced polymer composites. Biochar was produced from waste orange peel particulates at different carbonization temperatures of 400 C, 600 C, and 800 C using the pyrolysis process. Composites were fabricated by incorporating biochar as filler material at varying weight percentages (10%, 15%, and 20%) into the polymer matrix. The erosive wear behaviour was evaluated using an air jet erosion test apparatus under different operating conditions, including impact angles (45 , 60 , and 90) and impact velocities (48, 70, and 82 m/s). An L27 orthogonal array based on Taguchi's method was employed to design the experiments. To enhance prediction accuracy and validate the optimized responses, ML models such as support vector machine, random forest (RF), and decision tree were developed. Among the ML models, the RF model exhibited the highest predictive performance with an R^2 value of 0.835 compared to other models. The results indicate that the erosive wear loss decreases with increasing carbonization temperature, with maximum erosion resistance observed in composites reinforced with biochar produced at 800 C.

Keywords Erosion wear · Biochar · Taguchi approach · Machine learning methods.

Introduction

Traditional composite materials reinforced with synthetic fibers such as glass fiber and carbon fiber are widely used in various industries, including automotive and household applications, due to their low weight, high specific strength, and stiffness[1–4]. However, these materials present significant challenges related to recyclability, reusability, and biodegradability after the end of their service life. Consequently, increasing environmental regulations have encouraged researchers to explore eco-friendly, sustainable, and cost-effective alternatives to

This Article in Press is shared early to give you faster access to new research. It is citable and carries a permanent DOI. The final edited version will replace it automatically.

Nankwaya Ntumba Zacharie is an Independent Researcher.

https://doi.org/10.1038/s41598-026-78201-1

Published online: 24 November 2026

scientific reports

synthetic fiber-based composites. In this context, bio-waste and natural fibers have gained considerable attention as potential reinforcement materials. Efficient recycling and utilization of waste materials not only help mitigate environmental pollution but also contribute to economic growth and job creation[5]. Nowadays, natural fiber plants such as jute, kenaf, sisal, coir, banana, and aloe vera, etc., in addition to bio-waste materials, are the center of attention for researchers and act as an alternative to conventional glass fiber composites[6–10].

Maximum failure occurs in various machines and structures due to wear; out of different types of wear, erosive wear is one of the most important types of wear occurs in composite materials. Several researchers have studied the erosive wear behaviour of natural fiber-reinforced polymer composites [11–13]. However, certain notable deficits of natural fiber properties, such as moisture absorption capacity, subsequent swelling and degradation, poor chemical and fire resistance, poor interfacial interaction with polymer matrix, and high dispersion of mechanical properties. To overcome these limitations, carbonization of natural fibers to produce biochar (CB) has emerged as a promising approach. Biochar exhibits several advantageous properties, including non-toxicity, high hardness, improved mechanical strength, corrosion resistance, optical properties, enhanced thermal conductivity, dimensional stability, and superior thermal stability[14–18] and also used for energy storage applications[19,20]. Researchers have explored the production of carbon-based materials from various bio-waste sources[21–23]. Traditionally, carbon products are derived from coke and coal tar, which are expensive and less sustainable[13,14]. Therefore, alternative sources such as rice husk[24], bamboo[25], oil palm waste[26], wood apple and coconut shells[27], and palm kernel[28] have been utilized to produce carbon black due to their low cost and wide availability.

Carbon-based composites derived from such materials exhibit improved strength-to-weight ratio, lower density, and enhanced biodegradability[23,24]. Furthermore, the higher carbon content enhances the hydrophobic nature of the composites. The properties of biochar can be further improved by controlling the carbonization temperature during thermal treatment[24–28]. Biochar materials have found applications in brake pads, heavy metal removal, and wastewater treatment[25,26]. Sutikno[29] demonstrated that biochar derived from coconut shells can replace graphite in brake friction materials. Ojha et al.[30] reported enhanced hardness in composites reinforced with biochar derived from wood apple shells. Samantarai et al.[31] observed improved wear resistance using rice husk-derived biochar. Betancourt et al.[32] reported enhanced wear resistance in phenolic composites due to carbon fiber addition. Further studies have highlighted the beneficial effects of biochar on composite properties. Mauro Giorelli et al.[33] observed a transition from brittle to ductile behavior in epoxy composites reinforced with biochar derived from maple wood. Minugu et al.[34] reported a 52% improvement in erosion resistance with bael shell-derived biochar. Johnson et al.[35] achieved a 68.25% enhancement in erosion resistance using sawdust-derived biochar. Sundarakannan et al.[36] found that 10 wt.% PET biochar composites exhibited improved wear resistance. Li et al.[37] studied the effect of carbonization temperature on the mechanical properties of bamboo-derived biochar composites. Panchal et al.[38] reported significant improvement in wear resistance using activated carbon epoxy composites, with an enhancement of about 106%[39].

The feasibility of replacing conventional graphite with biochar in mineral grease formulations was explored in[40], and their findings showed that biochar can serve as a sustainable alternative lubricant additive while maintaining desirable tribological and rheological characteristics. Recent studies have shown that biochar obtained from agricultural waste can effectively enhance the mechanical performance of polymer composites[41]. The influence of walnut shell-derived biochar on vegetable-based lubricating greases improves the tribological performance of the bio-lubricant, highlighting the potential of biomass-derived carbon materials in lubrication applications[42]. Based on the literature, incorporation of CB filler into epoxy matrices significantly improves mechanical and tribological properties, with optimal performance typically observed at higher carbonization temperatures (around 800 C)[43,44]. Previous studies by Naik et al.[45,46] demonstrated that the tribological performance of polymer composites improves with the addition of orange peel powder (OPP), with optimal results obtained at 20 wt.% filler loading. Therefore, the primary objective of the present study is to investigate the effect of carbonization temperature on the erosive wear behavior of CB-reinforced epoxy composites derived from orange peel particulate.

The second objective is to further analyze and predict the experimental wear loss results using machine learning techniques, which have emerged as important tools in modern engineering research [47,48] due to their capability to capture complex and nonlinear relationships between input parameters and output responses [49]. In recent years, ML approaches have been extensively applied across thermal systems[50], energy applications[51,52] e.t.c for accurate prediction and optimization of system performance, and also, an investigation on the tribological performance of PLA/rice husk biochar composites was carried out by integrating response surface methodology with machine learning models[53]. In machining and tribological applications, traditional empirical and analytical models are often limited in their ability to represent the intricate interactions among process variables. Therefore, ML models provide a reliable tool by providing accuracy in prediction and reducing dependency on extensive experimental trials. In the present study, ML algorithms such as SVR [54], RF[55], and DT[56] are implemented to predict the erosion wear (EW) behavior based on input parameters such as impact velocity (IV), carbonization temperature (CT), impact angle (IA), and filler percentage (FP). These models facilitate efficient data analysis, enhance prediction capability, and provide a robust framework for optimizing process parameters in biochar-reinforced polymer composites.

Although several studies have investigated the mechanical and tribological performance of biochar-filled polymer composites, most have primarily focused on experimental characterization or statistical optimization independently. Studies integrating process optimization with machine learning for predictive modeling of erosion behavior remain scarce, particularly for biochar derived from agricultural waste. In the present work, orange-peel biochar produced at different carbonization temperatures is employed as a sustainable reinforcement in epoxy composites, and its erosion behaviour is systematically evaluated using a Taguchi experimental design. The experimental observations are further integrated with machine learning models through a physics-constrained synthetic data generation strategy confined to the experimentally investigated design space, enabling reliable prediction of wear behavior while addressing the limitations associated with small experimental datasets. This unified framework establishes a direct connection between biochar processing, erosion performance, statistical optimization, and data-driven prediction, thereby providing a comprehensive methodology for the design and analysis of sustainable polymer composite systems.

Materials and methods

In this work, natural CB was used as a filler material to fabricate the composite. Epoxy resin (Araldite LY556) and hardener (HY951) were used for the preparation of the polymer composite. The epoxy matrix belongs to the epoxide family, commonly known as bisphenol-A diglycidyl ether.

Preparation of CB

Carbonization has a positive impact on the mechanical and tribological properties of natural fibers. However, achieving significant improvement in polymer composite properties using natural fibers as reinforcement is challenging due to the presence of pores, impurities, and moisture introduced during extraction. The selection of raw material for producing CB depends on its composition. Lignocellulosic fibers mainly consist of cellulose, hemicellulose, and lignin, and the characteristics of hard shell materials are governed by their relative proportions. Orange peel (OP) contains cellulose, hemicellulose, lignin, proteins, and a certain amount of carbohydrates[32].

From the literature review[57–59], it has been observed that the physicochemical changes of lignocellulosic fiber occur within the temperature range of 400 C to 800 C. The retention of oxygen-containing functional groups was observed at low carbonization temperatures, i.e., 400 C, whereas devolatilization occurs in the range of 600 C carbonization temperature, and there is a possibility of increased aromaticity. However, the biochar developed at 800°C carbonization temperature contains a highly carbonized and porous structure with enhanced thermal stability and porous content. The temperature beyond 800 C has not been considered because the changes in biochar

characteristics are often relatively small compared with substantially higher energy requirements and processing costs. In the present study, orange peel powder (OPP) collected from the local market was used to produce CB filler material. Three types of CB, labeled as CB4, CB6, and CB8, were produced through the pyrolysis process at carbonization temperatures of 400 C, 600 C, and 800 C, respectively. The heating rate was maintained at 5 C/min, and the samples were kept in the furnace for 2 h under an inert atmosphere. The complete procedure for obtaining CB from OPP is illustrated in Fig. 1.

Composite laminate fabrication

The composite specimens were fabricated using the hand lay-up technique with a wooden mould of dimensions $160 \times 60 \times 6$ mm. A mould-releasing spray (heavy-duty silicone spray) was applied to the inner surface of the mould to facilitate easy removal of the samples. A mixture of epoxy and hardener was prepared in a weight ratio of 10:1 and thoroughly mixed. The mixture was then placed in a vacuum chamber to eliminate entrapped air bubbles. Subsequently, different CB filler materials were added and mixed thoroughly to ensure homogeneous distribution. The mixture was then poured into the mould.

A load was applied on the top surface of the mould, and the composite was allowed to cure at room temperature for 48 h. Due to the applied load, a small amount of mixture may have been expelled from the mould; however, care was taken to maintain a uniform thickness. Specimens of dimensions $25 \times 25 \times 6$ mm^3 were cut from the composite slab using a diamond cutter for erosion testing. Adequate care was taken to maintain a constant thickness of 6 mm for all samples.

Erosive wear test set-up and mechanism

The erosive wear behavior of the specimens was studied using a solid particle erosion test rig in accordance with the ASTM G76-95 standard. Experiments were conducted at different pressures, which were controlled using a pressure regulator attached to the test rig. Before testing, samples were cleaned with acetone and weighed using a precision electronic balance with an accuracy of 0.001 g to determine weight loss. Each sample was fixed in the erosion test rig at the desired impingement angle and subjected to erosion for 10 minutes[45]. The weight loss (W_m) was calculated as the difference between initial and final weights. The erosion rate (E_r) was determined using:

$$E_r = \frac{\text{Weight loss due to erosion}}{\text{Weight of erodent supplied}} \tag{1}$$

The weight of the eroded material supplied was calculated as:

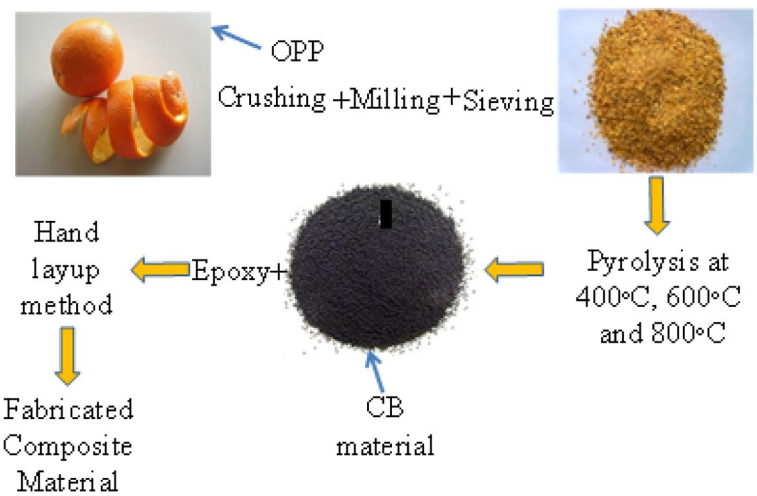

Fig. 1 Procedure for preparation of CB from OPP.

Table 1 Operating parameters for erosive wear experiment[45].

Component	Parameter	Unit
Erodent	Silica sand	–
Average erodent size	150–250	μm
Erodent shape	Irregular, slightly rounded	–
Impact angle (α)	30, 45, 60, 90	
Erodent velocity (v)	48, 70, 82	m/s
Feed rate of erodent	2 ± 0.02	g/min
Experiment temperature	Ambient	C
Distance from nozzle	10	mm
Nozzle diameter	4	mm

Table 2 Selected parameters and their levels for erosion trials.

Impact velocity (m/s)	Impact angle ( )	Filler (%)	Carbonization temperature (C)
48	45	10	400
70	60	15	600
82	90	20	800

$$\text{Weight of erodent} = \text{Testing time} \times \text{Particle feed rate}$$

For each test condition, five samples of identical dimensions were tested under the same operating conditions. The operating parameters are listed in Table 1.

Microscopic analysis

A scanning electron microscope (SEM) was used to examine the morphological characteristics of OPP-derived carbon particulates. Prior to analysis, the CB particulates were gold-coated to ensure smooth electron conduction during imaging. Energy dispersive spectroscopy (EDS) analysis of both raw and carbonized OPP was performed using a Bruker Nano Model XFlash Detector 5030 to identify the elemental composition of the samples. For EDS analysis, the particulates were coated with a thin layer of platinum to facilitate the smooth passage of high-energy electron beams through the material.

Taguchi's orthogonal array

Taguchi's orthogonal array is a powerful optimization tool used to minimize the number of experimental trials while effectively analyzing the influence of control parameters on output response. In the present study, the objective is to investigate the influence of impact velocity (IV), impact angle (IA), filler percentage (FP), and carbonization temperature (CT) on the erosion behavior of biochar-reinforced polymer composites. The selected control parameters and their levels are listed in Table 2. A full factorial design would require $4^3 = 64$ experimental runs, which is both time-consuming and costly. Therefore, an L27 orthogonal array based on Taguchi's design was employed, reducing the total number of experiments to 27. This significantly decreases experimental effort while maintaining analytical accuracy (see Table 3).

Taguchi analysis categorizes experimental observations based on the signal-to-noise (S/N) ratio, where the signal represents desirable values and noise represents undesirable variations. Since a lower wear loss is desired, the "lower-the-better" criterion is applied. The S/N ratio is calculated using the logarithmic loss function as:

$$\text{S/N} = -10 \log_{10} \left(\frac{1}{n} \sum_{i=1}^{n} Y_i^2 \right) \tag{2}$$

where Y_i is the observed value and n is the number of observations.

Table 3 Experimental results using Taguchi L27 orthogonal array.

SL no.	IV	FP	IA	CT	EW	S/N	Mean
1	48	10	45	400	2.430	− 7.7121	2.430
2	48	15	45	400	3.028	− 9.6231	3.028
3	48	20	45	400	1.774	− 4.9791	1.774
4	48	10	60	600	1.642	− 4.3075	1.642
5	48	15	60	600	1.513	− 3.5968	1.513
6	48	20	60	600	1.095	− 0.7883	1.095
7	48	10	90	800	1.952	− 5.8096	1.952
8	48	15	90	800	1.609	− 4.1311	1.609
9	48	20	90	800	1.103	− 0.8515	1.103
10	70	10	60	400	3.181	− 10.0513	3.181
11	70	15	60	400	3.281	− 10.3201	3.281
12	70	20	60	400	3.228	− 10.1787	3.228
13	70	10	90	600	2.126	− 6.5513	2.126
14	70	15	90	600	2.685	− 8.5789	2.685
15	70	20	90	600	2.250	− 7.0437	2.250
16	70	10	45	800	2.143	− 6.6204	2.143
17	70	15	45	800	1.843	− 5.3105	1.843
18	70	20	45	800	1.858	− 5.3809	1.858
19	82	10	90	400	5.050	− 14.0658	5.050
20	82	15	90	400	4.259	− 12.5862	4.259
21	82	20	90	400	3.914	− 11.8524	3.914
22	82	10	45	600	3.494	− 10.8665	3.494
23	82	15	45	600	3.337	− 10.4671	3.337
24	82	20	45	600	2.355	− 7.4398	2.355
25	82	10	60	800	3.730	− 11.4342	3.730
26	82	15	60	800	2.806	− 8.9618	2.806
27	82	20	60	800	1.666	− 4.4335	1.666

Machine learning methodology

In engineering applications, machine learning (ML) models play a crucial role in predicting the EW behavior of materials. In the present study, EW is influenced by several input features, namely IV, CT, IA, and FP. These parameters are used as input features in the ML models, while wear loss is considered the output response. To predict the output response from the given input features, three ML algorithms were employed: SVR, RF, and DT. Due to the high cost associated with wear testing, the availability of large experimental datasets is often limited. Therefore, synthetic data was generated from experimental data while preserving the underlying physical behavior of the material.

Initially, a second-order polynomial response surface model (RSM) was developed to establish the relationship between input features (IV, CT, IA, FP) and the output response (EW). Subsequently, Gaussian process regression (GPR) combined with latin hypercube sampling (LHS) was used to generate synthetic data within the convex hull of the experimental design space. No extrapolation beyond the experimental limits was performed to ensure the preservation of physical trends between input features and output response. The generated synthetic dataset was used to train the ML models. The trained models were then tested using experimental data to evaluate their predictive capability for EW. The overall workflow of the ML model is illustrated in Fig. 2.

To improve the learning capability of the machine learning models and reduce the variance associated with the limited experimental dataset, synthetic samples were generated using GPR. The original dataset consisted of 27 experimental observations obtained from the Taguchi L27 orthogonal array, which served as the foundation for constructing the surrogate model. After training the GPR model using only the experimental data, a total of 500 synthetic samples were generated within the experimentally investigated design space. Consequently, the ML

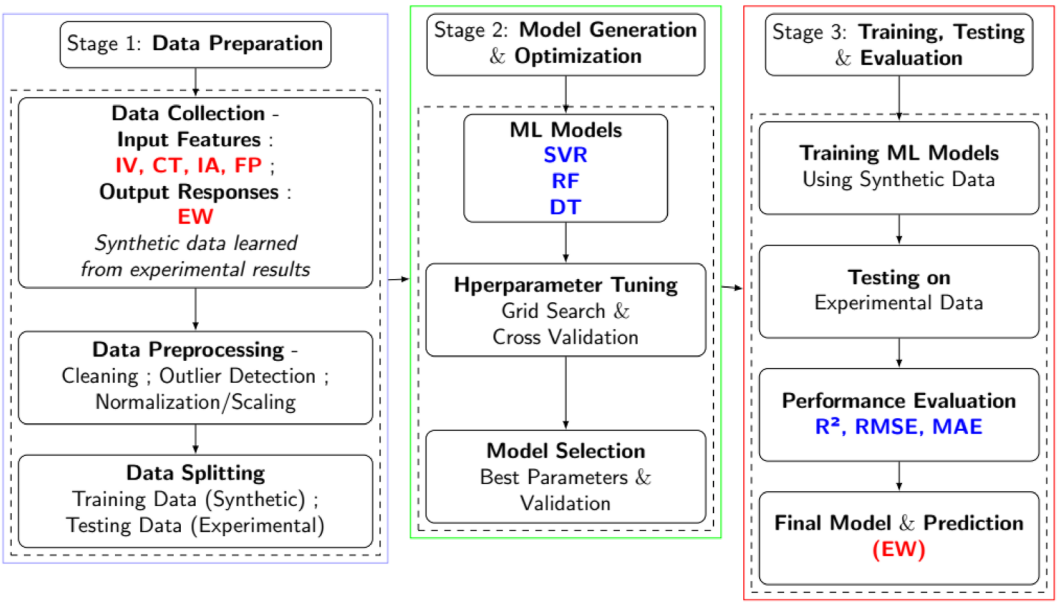

Fig. 2 Machine learning workflow for predicting EW using input features (IV, CT, IA, FP).

Table 4 Statistical validation of the experimental and GPR-generated synthetic wear-loss datasets.

Statistical metric	Experimental	Synthetic
Mean wear loss	2.5173	2.3424
Standard deviation	0.9960	0.7580
Skewness	0.5940	0.8983
Kurtosis	2.7742	4.2664
Statistical hypothesis testing		
Kolmogorov–Smirnov statistic	0.1783	
Kolmogorov–Smirnov *p*-value	0.3167	
Mann–Whitney U *p*-value	0.4751	

models were trained using a synthetically generated dataset and tested on an experimental dataset. To maintain the physical validity of the generated dataset, synthetic samples were produced exclusively within the minimum and maximum limits of each experimental variable, including IV, IA, FP, and CT. No extrapolation beyond the experimentally investigated parameter space was permitted. Since GPR performs probabilistic interpolation based on experimentally observed responses, the generated samples preserve the nonlinear relationships learned from the original experiments while remaining consistent with the physical trends exhibited by the measured data. The generated dataset was further examined to ensure that the response values remained within the experimentally observed range and did not introduce unrealistic response behavior.

The synthetic dataset was employed solely to improve the learning efficiency and generalization capability of the machine learning algorithms. Model performance was ultimately evaluated using the experimentally measured observations, ensuring that the reported predictive accuracy reflected agreement with actual experimental data rather than the generated samples. This strategy improves model robustness while preserving the physical consistency of the experimental system.

The statistical consistency between the experimental and GPR-generated synthetic datasets was evaluated to verify that the synthetic samples adequately preserved the characteristics of the experimentally observed wear-loss response. As summarized in Table 4, the synthetic dataset exhibits statistical properties comparable to those of the experimental observations, with similar measures of central tendency and variability. Furthermore, the Kolmogorov–Smirnov (KS) test ($p = 0.3167$) and Mann–Whitney U test ($p = 0.4751$) indicate that no statistically

significant differences exist between the two datasets at the 95% confidence level. These results demonstrate that the synthetic samples remain statistically consistent with the experimental data while being generated entirely within the investigated design space, thereby providing a reliable dataset for training the machine learning models without introducing extrapolation beyond the experimental conditions.

To obtain the optimal predictive performance of the machine learning models, a systematic hyperparameter optimization procedure was essential[60,61] and therefore carried out using exhaustive grid search combined with k-fold cross-validation. For each candidate model, several combinations of hyperparameters were evaluated, and the set that produced the best cross-validation performance was selected for final model development. The SVR model was implemented with a radial basis function (RBF) kernel, and its optimized hyperparameters were a regularization parameter of C = 100, a kernel coefficient of $\gamma = 0.03$, and an insensitive loss parameter of $\varepsilon = 0.005$. The RF model was optimized using 500 decision trees, a maximum tree depth of 8, a minimum samples split value of 2, a minimum samples leaf value of 1, and the square root of the number of features as the maximum number of features considered at each split. The DT model was optimized using grid search with cross-validation by tuning the splitting criterion (squared_error and absolute_error), the maximum tree depth (1, 2, 4, and 8) and the minimum number of samples required at each leaf node (1–5). These optimized hyperparameter values were used in the final predictive models to ensure robust performance and reproducibility.

The RSM employed for synthetic data generation serves as an intermediate approximation of the experimentally observed response and is not intended to replace physical experiments or the final machine learning models. As a second-order polynomial formulation, the RSM may not fully capture highly nonlinear interactions among the machining parameters. Consequently, any modeling error inherent to the RSM could propagate into the generated synthetic dataset. To minimize this limitation, synthetic samples were generated exclusively within the experimentally investigated design space without extrapolation beyond the measured parameter limits. In addition, statistical validation confirmed good agreement between the experimental and synthetic datasets, and the developed machine learning models were evaluated solely using experimentally measured wear-loss values. Therefore, the reported predictive performance reflects consistency with experimental observations while recognizing the inherent limitations associated with RSM-based data augmentation.

To improve the learning capability of the machine learning models under a limited experimental dataset, 500 synthetic samples were generated using Gaussian process regression (GPR) combined with latin hypercube sampling (LHS) within the experimentally investigated parameter ranges. These generated samples were used exclusively for model training, whereas the experimentally measured wear-loss values were reserved for independent model evaluation. This strategy avoids direct reuse of the generated samples during performance assessment and reduces the possibility of data leakage between the training and validation stages. Since the experimental dataset consisted of only 27 observations, the potential risk of model overfitting cannot be eliminated. However, restricting the synthetic data generation to the experimentally investigated design space, together with statistical validation of the generated dataset and independent evaluation against experimental measurements, helps improve the robustness and reliability of the developed machine learning models. Nevertheless, future investigations incorporating larger experimental datasets are expected to further improve the generalization capability of the proposed predictive framework.

To enhance the learning capability of the machine learning models while preserving the integrity of the experimental observations, a total of 500 synthetic samples were generated within the experimentally observed design space using the GPR-LHS framework. These synthetic samples were used exclusively for training the SVR, RF, and DT models. The 27 experimental observations obtained from the Taguchi L_{27} orthogonal array were not included in the training process; instead, they were retained as an independent test dataset to evaluate the predictive performance of the developed models. Hyperparameter optimization was performed using grid search coupled with five-fold cross-validation on the synthetic training dataset, while a fixed random seed of 42 was employed to ensure reproducibility of the model development process. The complete details are provided in Table 5 for reference.

Table 5 Summary of the machine learning training and validation strategy.

Parameter	Description
Training dataset	500 synthetic samples generated using the GPR–LHS framework
Testing dataset	27 experimental observations (Taguchi L_{27} orthogonal array)
Hyperparameter optimization	Grid search with five-fold cross-validation
Random seed	42
ML models	SVR, random forest (RF), decision tree (DT)

The performance of the ML models was evaluated using three statistical metrics: coefficient of determination (R^2), root mean square error (RMSE), and mean absolute error (MAE), as defined in Eqs. (3–5).

$$R^2 = 1 - \frac{\sum_{j=1}^{m} (\hat{q}_j - q_j)^2}{\sum_{j=1}^{m} (q_j - \bar{q})^2} \tag{3}$$

$$\text{RMSE} = \sqrt{\frac{1}{m} \sum_{j=1}^{m} (q_j - \hat{q}_j)^2} \tag{4}$$

$$\text{MAE} = \frac{1}{m} \sum_{j=1}^{m} |q_j - \hat{q}_j| \tag{5}$$

where m represents the number of test samples, q_j is the experimental measured EW value for the jth sample, $\hat{q}_j$ is the predicted value obtained from the ML model, and $\bar{q}$ is the mean of the experimental EW values.

The predictive performance of the SVR, RF, and DT models was evaluated by comparing their predicted erosive wear values with the corresponding experimental observations. The R^2, RMSE, and MAE were calculated based on these comparisons. Since the original experimental observations were also used to train the GPR model for synthetic-data generation, the reported metrics should be interpreted in the context of this dependence and not as a fully independent evaluation on unseen experimental data which is the limitation of the present work.

Results and discussion

Microstructural analysis

Figure 3 shows the SEM analysis of raw OPP and CB filler materials prepared at different carbonization temperatures. The raw OPP appears dense with almost no visible porous structure, as shown in Fig. 3a. In contrast, a porous structure is clearly observed on the surface of CB4 due to the removal of volatile components during carbonization (Fig. 3b). With increasing carbonization temperature, the diameter of CB particles decreases, while the volume of microporous structures increases. This is evident in CB6 (Fig. 3c), where an enhanced porous surface area is observed. A highly developed porous structure is seen in CB8 (Fig. 3d), attributed to the removal of a larger amount of volatile matter. Consequently, CB8 exhibits a more developed porous morphology structure than CB4 and CB6, which is expected to influence the composite properties. However, quantitative surface area and adsorption measurements were not performed in the present study.

The EDX spectra of CB filler materials and the corresponding elemental composition are presented in Fig. 4. The results indicate that the carbon content increases with increasing carbonization temperature. The increased carbon content suggests that the resulting composite materials can sustain higher loads, exhibit improved mechanical stability, and maintain a lower overall weight.

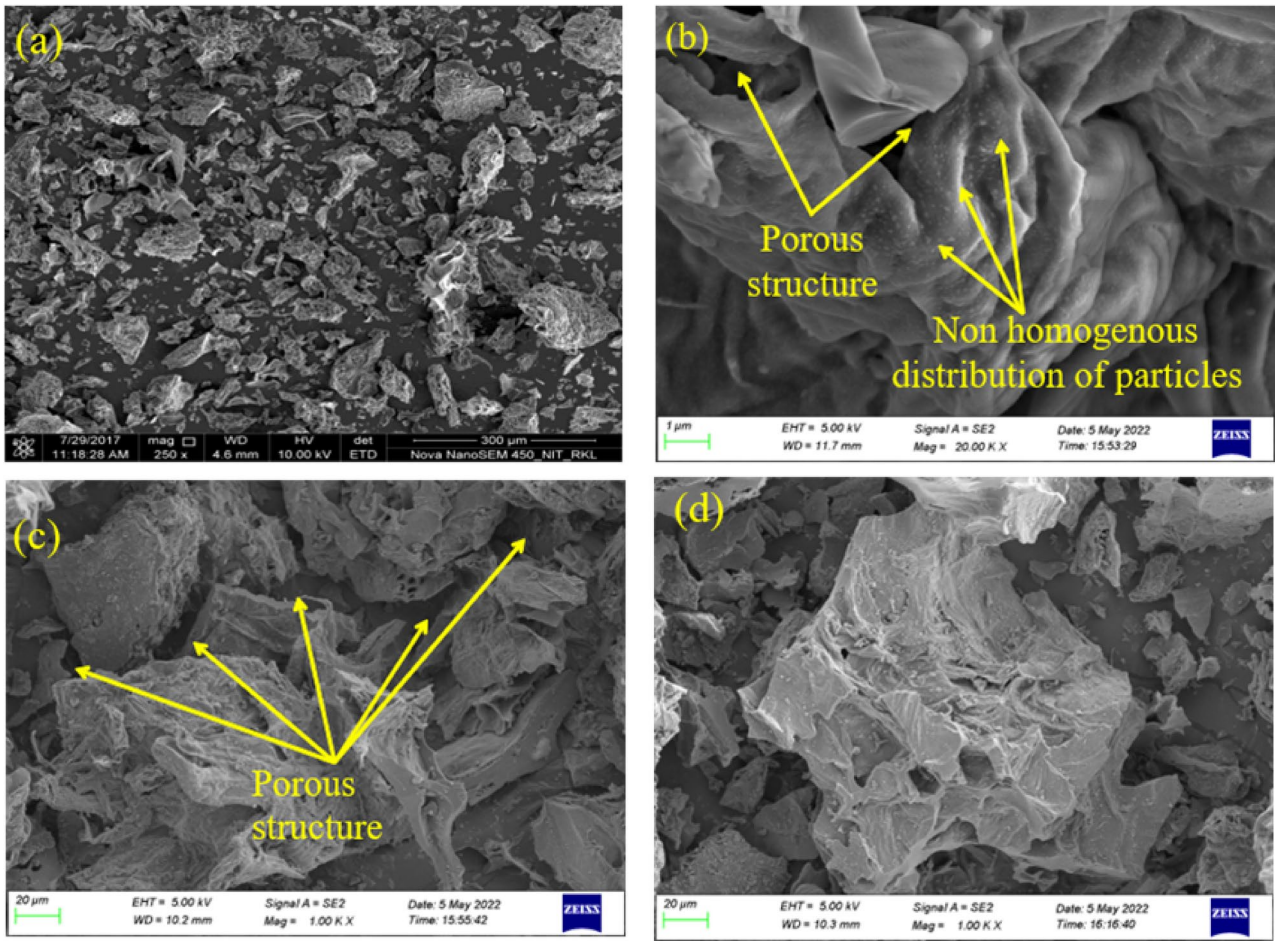

Fig. 3 SEM analysis of samples: (**a**) Pure OPP, (**b**) CB4 (400 C), (**c**) CB6 (600 C), and (**d**) CB8 (800 C).

ANOVA for erosive wear

Analysis of variance (ANOVA) was used to evaluate the significance of process parameters affecting the EW rate, which include IV, CT, IA, and FP. This technique was analyzed at a confidence level of 95% and a significance level of 5%. The results of the ANOVA analysis for erosion rate are presented in Table 6. A larger F-value and a smaller P-value (< 0.05) indicate that the parameter is a statistically significant process parameter. The results show that IV is the most significant parameter, contributing 45.17% to the erosion rate, followed by CT (32.55%) and FP (10.09%). The IA shows a negligible effect (2.1%). The error percentage is very low (1%), indicating good model accuracy. The regression equation for EW rate, utilizing Minitab 18 statistical software, is expressed in Eq. (6).

$$EW = 2.062 + 0.04546\,IV - 0.003176\,CT + 0.00717\,IA - 0.0723\,FP \tag{6}$$

The adjusted R^2 for the regression model of erosion rate is 0.89, indicating a strong correlation between the predicted value from Eq. (6) and experimental results. Table 6 further confirms that IV, CT, and FP are the significant factors that mainly contribute to the EW rate.

Model summary: $R^2 = 89.99\%$, $R^2_{adj} = 85.54\%$, $R^2_{pred} = 77.47\%$.

Recent investigations have demonstrated that incorporating interaction effects and quadratic response models can improve the characterization of complex nonlinear relationships in manufacturing processes, thereby

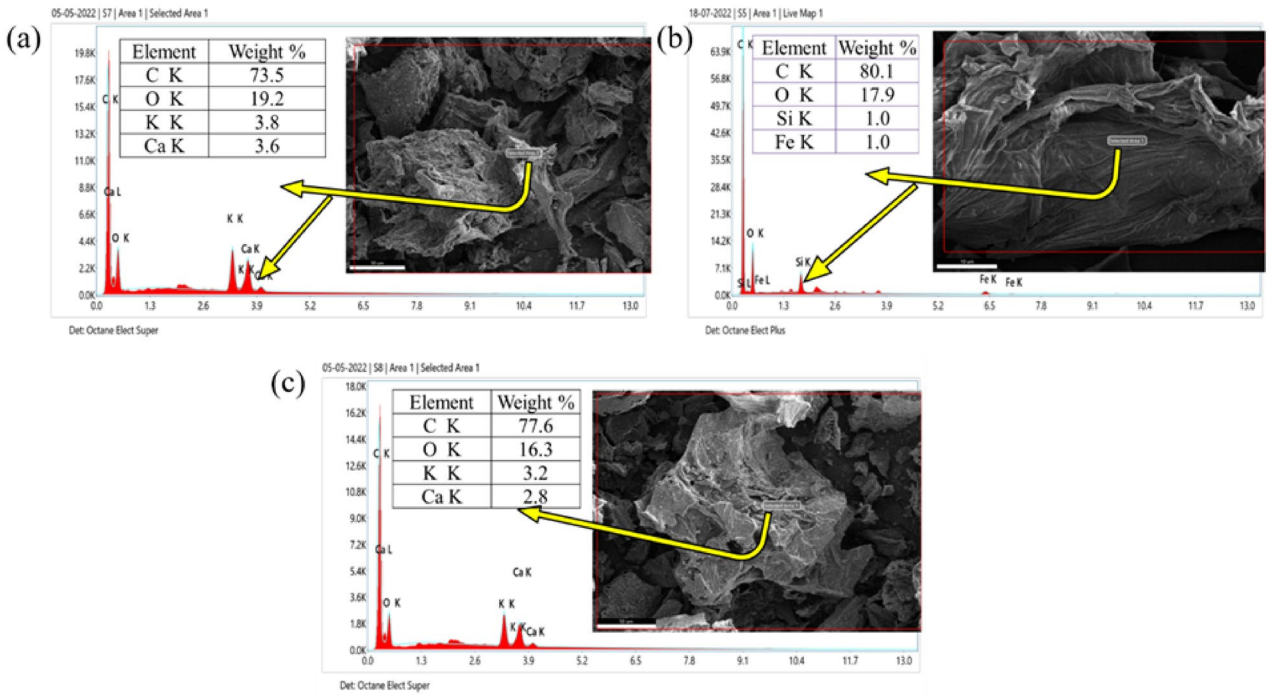

Fig. 4 EDX analysis of samples: (**a**) CB4 (400 C), (**b**) CB6 (600 C), and (**c**) CB8 (800 C).

Table 6 ANOVA results for erosive wear.

Source	DF	Adj SS	Adj MS	F-Value	P-Value
IV	2	11.6697	5.8349	45.17	0.000
CT	2	8.4088	4.2044	32.55	0.000
IA	2	0.5594	0.2797	2.10	0.172
FP	2	2.6086	1.3043	10.09	0.002
Error	18	2.5867	0.1437		
Total	26	25.8331			

Table 7 Response table for S/N ratios (smaller is better).

Level	IV	CT	IA	FP
1	− 4.644	− 10.152	− 7.600	−8.602
2	− 7.782	− 6.627	− 7.119	−8.175
3	− 10.234	− 5.882	− 7.941	−5.883
Delta	5.590	4.271	0.822	2.719
Rank	1	2	4	3

enhancing predictive capability and process optimization[62]. Motivated by these findings, future work will focus on extending the present framework to include higher-order regression formulations alongside machine learning models for a more comprehensive analysis of parameter interactions.

S/N ratio analysis

The influence of process variables such as IV, CT, IA, and FP on erosive wear (EW) is analyzed using the (S/N) ratio. The optimal condition corresponds to the highest S/N ratio with minimal variance. The difference between the maximum and minimum mean S/N ratio values (delta) indicates the relative influence of each parameter. Tables 7 and 8 present the response tables for S/N ratios and mean values, respectively. Based on delta values,

Table 8 Response table for means.

Level	IV	CT	IA	FP
1	1.794	3.349	2.474	2.861
2	2.511	2.277	2.460	2.707
3	3.401	2.079	2.772	2.138
Delta	1.607	1.271	0.312	0.723
Rank	1	2	4	3

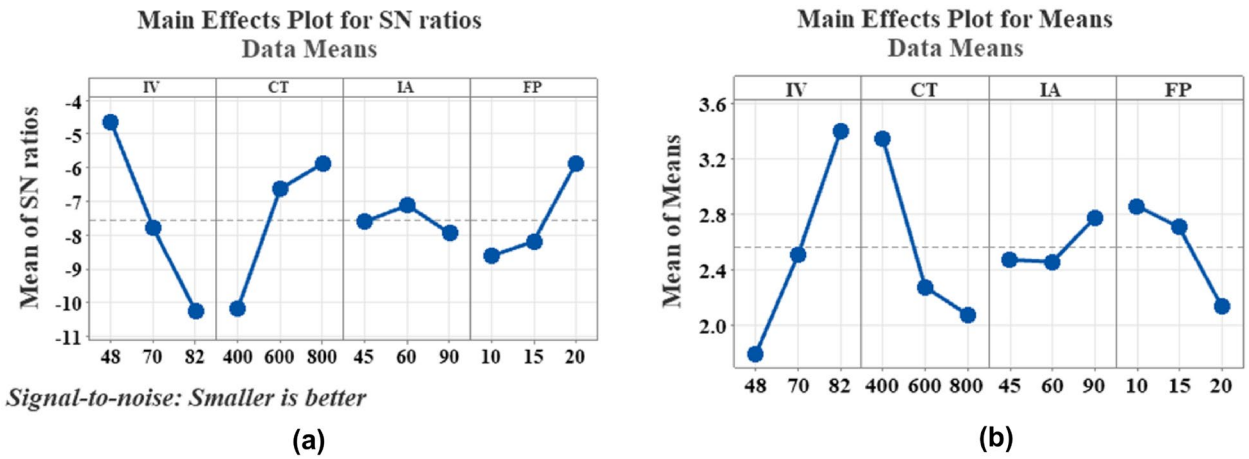

Fig. 5 (**a**) Main effects plot for S/N ratio and (**b**) Main effects plot for means.

impact velocity is the most influential parameter, followed by carbonization temperature and filler percentage, whereas impact angle shows the least influence. The EW rate decreases with increasing carbonization temperature, reaching an optimum at 800 C. This is attributed to the formation of porous structures and increased carbon content, as confirmed by SEM and proximate analysis. The improved erosive wear resistance may be associated with the more porous morphology and higher carbon content of the biochar produced at higher carbonization temperatures. However, the interfacial bonding was not quantitatively evaluated in the present study, and therefore, no direct conclusion regarding bond strength is made.

Both the main effect plots for means and S/N ratios are shown in Fig. 5. A steep slope indicates a strong influence of a parameter, whereas a flat slope indicates minimal effect. Impact velocity exhibits the strongest influence, while impact angle shows the least effect. The optimal parameter combination for minimum wear is IV = 48 m/s, IA = 60 , FP = 20 wt.%, and CT = 800 C. Increasing CT and FP improves wear resistance, while higher IV (82 m/s) leads to increased wear.

Residual analysis

Residual analysis is a crucial process in validating statistical models, ensuring all fundamental criteria such as normality, homoscedasticity, independence, and linearity are satisfied. This research analyzes the residual behavior of the developed model, which includes four testing plots such as the normal probability plot, residuals versus fitted values plot, histogram of residuals, and residuals versus observation order plot. These evaluations provide insight into the model's validity and the reliability of the resulting statistical inferences. The normal probability plot (Fig. 6a) illustrates that the residuals align closely with the reference line, indicating that they are approximately normally distributed. Minor deviations at the extremes may suggest slight skewness, likely attributable to experimental variability. The assumption of normality is sufficiently satisfied, enabling valid statistical inference. The residuals versus fitted value plot (as shown in Fig. 6b) is used to evaluate the existence of autocorrelation or sequential dependency in the residuals. In optimal conditions, residuals should present unstructured randomness,

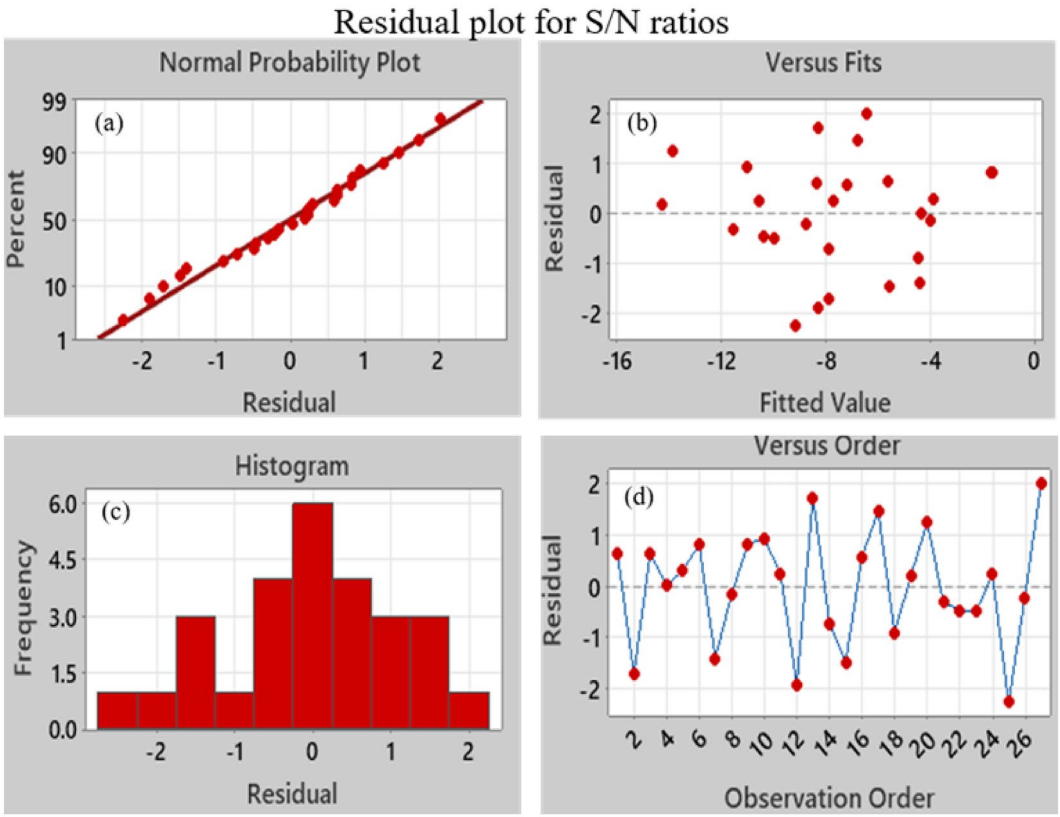

Fig. 6 Residual analysis: (**a**) Normal probability plot, (**b**) Residual vs fitted values, (**c**) Histogram, (**d**) Residual vs order.

with no clear trends or sequential dependencies. The residuals shown in the plot exhibit unpredictable fluctuations. In the absence of a systematic pattern, it can be concluded that the residuals display independence, suggesting that autocorrelation issues do not affect the model. The histogram displays a curve that closely resembles a bell-shaped distribution as shown in Fig. 6c, suggesting that the residuals follow a normal distribution. No noticeable skewness or multimodal patterns were present, suggesting that the residuals show minimal deviations from normality. The distribution of the residuals closely aligns with a normal distribution, which supports the results observed in the normal probability plot. The normality assumption is adequately fulfilled, which further supports the reliability of the statistical model. The residuals should be independent of one another, meaning no systematic pattern over time. The residuals versus order plot (as shown in Fig. 6d) shows fluctuations; however, no obvious trend or cyclic pattern. This error is insignificant and can be considered negligible. The presence of a pattern would indicate autocorrelation, meaning the residuals are dependent on previous values. Consequently, the residuals exhibit independence, indicating that no time-dependent or sequential factors are distorting the analysis.

Surface plot analysis

The 3D surface plot illustrates the interaction between variables and helps to determine the optimal parameter conditions to reduce EW. The research plays a vital role in the design of materials capable of withstanding erosion in harsh environmental conditions. A non-linear, saddle-like surface configuration is observed, highlighting the intricate relationship between CT and IV as shown in Fig. 7a. An inverse relationship between CT and EW is observed at lower IV values, indicating that with an increase in carbonization, erosion resistance improves through structural transformations. When IV is elevated, increasing CT tends to increase EW, potentially due to increased brittleness or failure modes activated under high IV. Hence, it is evident that IV plays a more dominant role in

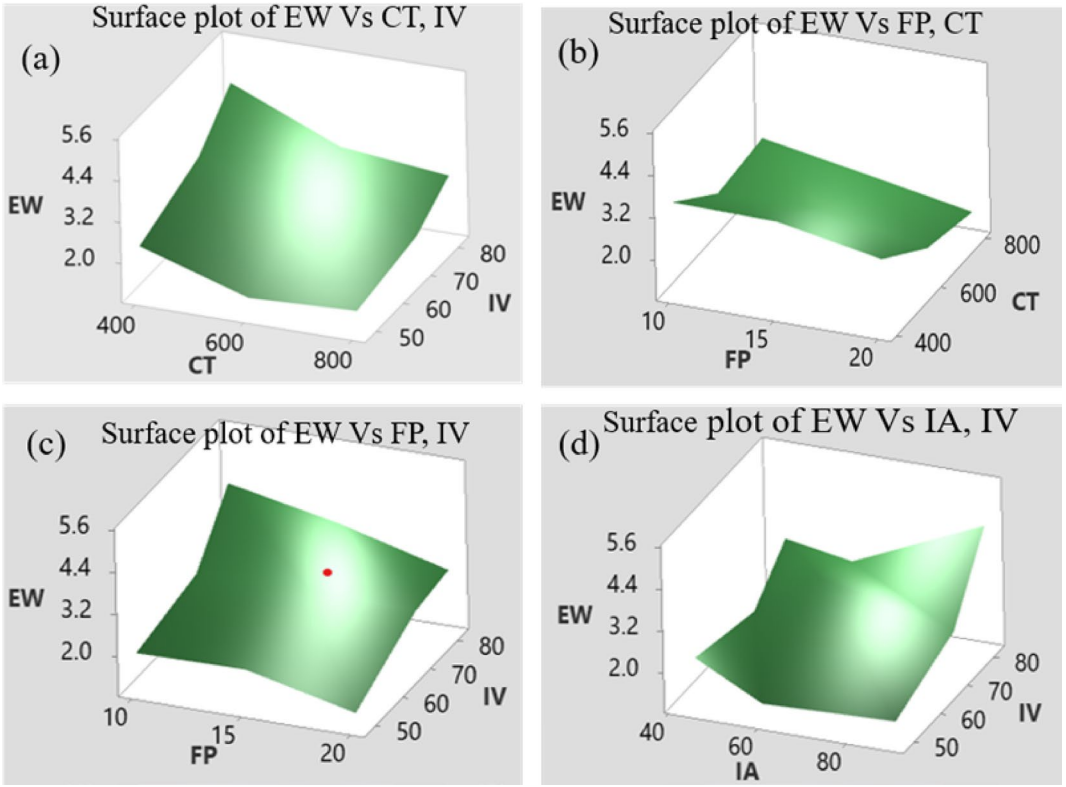

Fig. 7 Surface plots showing interaction effects: (**a**) IV vs CT, (**b**) CT vs FP, (**c**) IV vs FP, (**d**) IV vs IA.

comparison to CT. The Taguchi analysis confirms the same trend (S/N ratios). The response surface indicates a reduction in erosive wear in the intermediate carbonization temperature region under specific combinations of impact velocity. However, considering the combined effects of all process parameters, the Taguchi optimization and confirmation experiment identified 800°C as the global optimum carbonization temperature for minimizing erosive wear. Figure 7b shows the relationship between CT, FP and EW. The illustration shows a smooth, slightly inclined surface, indicating a moderate influence of both CT and FP on EW. An increase in CT corresponds to a decrease in EW, particularly noticeable at higher levels of filler content. Elevated carbonization is associated with changes in biochar morphology and carbon content, which may contribute to the observed improvement in erosion resistance. Further quantitative characterization is required to establish the underlying mechanisms. The observed effect can be attributed to the presence of filler particles, which act as barriers to erosive forces and contribute to increased structural rigidity. The optimal erosion resistance is achieved in the combination of CT at about 800 C and an FP near 20%.

This investigation uses a surface plot to clarify the interaction between IV and FP and their collective impact on the composite's resistance to EW as shown in Fig. 7c. The EW increases with an increase in IV, particularly within the range of 50 m/s to 80 m/s. This effect is due to the elevated kinetic energy of particles at higher velocities, intensifying the impact forces and thereby increasing material loss. The gradient of the surface demonstrates that IV serves as a key factor influencing EW. An increase in FP from 10 to 20% results in a noticeable decrease in EW, indicating improved erosion resistance. The observed trend indicates that higher filler content improves erosion resistance through the incorporation of load-bearing particles and a consequent increase in surface hardness. At lower filler percentage (FP) levels, the matrix material may be more susceptible to impact pressures, resulting in increased wear. The combination of higher filler content and lower impact velocity yields the most effective erosion-resistant properties. As impact velocity increases from 50 m/s to 80 m/s across all impingement angles, EW exhibits a clear upward trend as shown in Fig. 7d. This behavior is explained by the elevated kinetic energy

of impacting particles, which facilitates greater momentum exchange and accelerates material removal. The IA has a non-linear effect on erosive wear. At lower IA, i.e. 40 –60 , EW remains relatively low, suggesting that the particles primarily glide across the surface, causing micro-cutting or ploughing. A substantial rise in EW is observed as the angle nears 90 , with the effect being more pronounced under higher IV. This indicates a transition in the wear mechanism from sliding-dominated (abrasive) wear to deformation and fracture-dominated (impact erosion) wear modes. The relationship between IV and IA is clearly illustrated in the plot. The highest EW occurs under the conditions of elevated impact velocity (80 m/s) and a high impact angle (90). This indicates a synergistic effect wherein the perpendicular impact of high-speed particles results in significant material damage via mechanisms including surface micro-cracking, spalling, and fragmentation. In contrast, minimal wear occurs at lower IV and moderate IA (approximately 60), indicating that a moderate angle of attack diminishes the normal component of impact force, which subsequently reduces the erosive effect.

Confirmation experiment

The design of experiments culminates in the confirmation test, which provides the success rate and reliability of the respective test. In this phase, the results derived from optimization and experiments are validated for accuracy, and any inconsistencies with the observations are recorded. The Taguchi optimization demonstrates that the IV1CT3FP3IA2 parameter shows optimal wear characteristics, a conclusion supported by the experimental results outlined in Table 9. The anticipated deviation of 3.36% between experimental and expected wear values suggests that the developed model is suitable for evaluating wear parameters with significant accuracy.

Second-order regression model

Although the first-order regression model adequately captured the overall trend in erosive wear, it assumes a linear relationship between the machining parameters and the response. To account for potential nonlinear effects and interactions among the process variables, a second-order regression model was subsequently developed. Compared with the first-order model, the quadratic regression equation incorporates curvature and interaction terms, thereby providing a more comprehensive representation of the experimental behaviour over the investigated design space. The developed quadratic regression equation for erosive wear (EW) is expressed as:

$$\begin{aligned} EW = {} & 6.19 - 0.0692\,IV - 0.01251\,CT - 0.0275\,IA + 0.340\,FP \\ & + 0.001225\,IV^2 + 0.000011\,CT^2 + 0.000212\,IA^2 - 0.00829\,FP^2 \\ & - 0.000030\,IV \times CT - 0.000012\,IV \times IA - 0.00160\,IV \times FP \\ & - 0.000121\,CT \times FP + 0.00025\,IA \times FP \end{aligned} \tag{7}$$

where EW is the erosive wear/mass loss (g), IV is the impact velocity (m/s), CT is the carbonization temperature (C), IA is the impact angle ( ), and FP is the filler percentage (wt%).

The second order regression equation indicates that erosive wear is governed by both linear and nonlinear effects of the process parameters. The negative linear coefficients of carbonisation temperature and impact angle indicate that increasing these parameters tends to reduce wear within the investigated range, while the quadratic terms account of curvature in the response. Likewise, the positive coefficient of IV^2 indicates a curvature in the response of erosive wear to impact velocity. Among the quadratic terms, only CT^2 was statistically significant ($p = 0.022$), whereas IV2 ($p = 0.074$), IA^2 ($p = 0.585$), and FP^2 ($p = 0.229$) were statistically insignificant. The

Table 9 Comparison of predicted and experimental wear loss.

Particulars	Initial	Prediction	Experimental
Level	$IV_1CT_3FP_3IA_2$	$IV_1CT_3FP_3IA_2$	$IV_1CT_3FP_3IA_2$
Wear loss	1.103	1.0462	1.0854
Error (%)	3.36		

interaction terms describe the combined influence of process parameters on erosive wear; however, none of the estimable interaction terms were statistically significant at the 5% significance level.

Analysis of variance of the quadratic regression model

The analysis of variance (ANOVA) for the developed second-order regression model is presented in the Table 10. The overall regression model was statistically significant ($F = 11.28$, $p < 0.001$), indicating that the developed quadratic model adequately represents the relationship between process parameters and erosive wear (EW). Among the process parameters, impact velocity (IV) contributed the highest proportion of the total variation (42.81%), followed by carbonization temperature (CT) with 28.12%, filler percentage (FP) with 9.1%, and impact angle (IA) with 1.88%. However, the individual linear effects of IV ($p = 0.452$), CT ($p = 0.115$), IA ($p = 0.667$) and FP ($p = 0.176$) were statistically insignificant at the 5% significance level. Thus, although IV showed the largest contribution among the individual linear terms, its contribution should be interpreted in terms of relative variation rather than statistical significance. The quadratic terms indicate the presence of nonlinear effects with in the investigated design space. Among quadratic terms, only the carbonized temperature squared term (CT^2) was statistically significant ($p = 0.022$), indicating a significant curvature effect of the carbonization temperature on erosive wear. The quadratic terms for impact velocity (IV^2, $p = 0.074$), impact angle (IA^2, $p = 0.585$) and filler percentage (FP^2, ($p = 0.229$) were statistically insignificant, at the 5% significance level. Nevertheless, their inclusion in the fitted second order model allows the nonlinear response behaviour to be represented over the investigated experimental domain.

The interaction effects did not show statistically significant effects at the 5% significance level. The p-values for IV×CT (0.632), IV×IA (0.982), IV×FP (0.255), CT×FP (0.316) and IA×FP (0.809) were all greater than 0.05, indicating that none of the estimable two factor interactions exerted a statistically significant effect on erosive wear with in the investigated design space. The CT×IA interaction was found to be not estimable for the present L27 experimental design and was therefore excluded from the fitted model.

The statistical indicators of the developed regression model are presented in Table 11. The model achieved an R2 of 91.85%, indicating the approximately 91.85% of the variation in erosive wear is explained by the fitted quadratic model. The adjusted R2 was 83.71%, while the predicted R2 was 59.29% indicating lower predictive performance for observations not included in the model fitting. The standard error (S) was 0.402320 and the PRESS value was 10.5170. The AICc and BIC values were 81.36 and 57.16 respectively. Overall, the statistically

Table 10 ANOVA results of the developed quadratic regression model for erosive wear (EW).

Source	DF	Seq SS	Contribution (%)	Adj SS	Adj MS	F-value	P-value
Regression	13	23.7289	91.85	23.7289	1.82530	11.28	0.000
IV	1	11.0597	42.81	0.0973	0.09734	0.60	0.452
CT	1	7.2644	28.12	0.4623	0.46230	2.86	0.115
IA	1	0.4857	1.88	0.0314	0.03141	0.19	0.667
FP	1	2.3508	9.10	0.3308	0.33080	2.04	0.176
IV × IV	1	0.6100	2.36	0.6100	0.60998	3.77	0.074
CT × CT	1	1.1444	4.43	1.1001	1.10008	6.80	0.022
IA × IA	1	0.0736	0.29	0.0506	0.05063	0.31	0.585
FP × FP	1	0.2578	1.00	0.2578	0.25778	1.59	0.229
IV × CT	1	0.0672	0.26	0.0390	0.03900	0.24	0.632
IV × IA	1	0.0001	0.00	0.0001	0.00009	0.00	0.982
IV × FP	1	0.2294	0.89	0.2294	0.22937	1.42	0.255
CT × FP	1	0.1759	0.68	0.1759	0.17593	1.09	0.316
IA × FP	1	0.0099	0.04	0.0099	0.00989	0.06	0.809
Error	13	2.1042	8.15	2.1042	0.16186	–	–
Total	26	25.8331	100.00	–	–	–	–

Table 11 Statistical performance indices of the developed quadratic regression model.

Model	S	R^2	Adjusted R^2	PRESS	Predicted R^2	AICc	BIC
Quadratic regression	0.402320	91.85%	83.71%	10.5170	59.29%	81.36	57.16

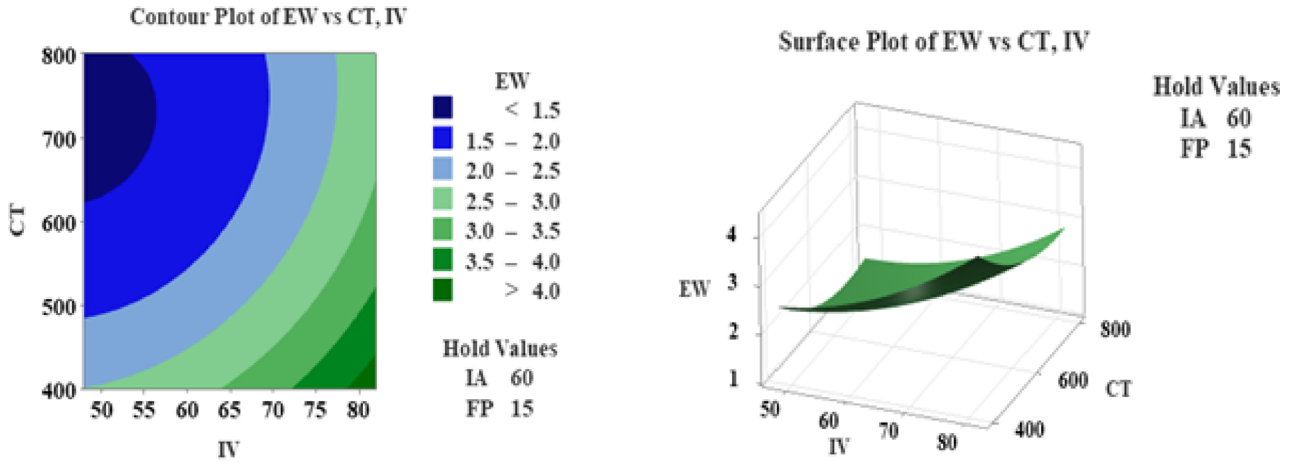

(a) Contour plot

(b) Three-dimensional response surface

Fig. 8 Response surface and contour plots illustrating the combined influence of impact velocity and carbonization temperature on erosive wear predicted by the developed quadratic regression model: (**a**) contour plot and (**b**) three-dimensional response surface.

significant regression model and high R2 value indicate that the fitted quadratic model capture a substantial proportion of the variation in the experimental erosive wear response.

Figure 8a,b presents the response surface and contour plots generated from the developed quadratic regression model. Both figures demonstrate the combined influence of impact velocity and carbonization temperature on erosive wear while keeping the remaining factors constant (IA = 60 and FP = 15). The curved response surface and curved contour lines indicate the nonlinear variation in erosive wear predicted by the quadratic regression model, with the carbonization temperature showing a statistically significant quadratic effect ($p = 0.022$). The minimum wear loss is observed in the region of low impact velocity (approximately 48–55 m/s) and high carbonization temperature (approximately 700–800 C). In contrast, erosive wear increases with increasing impact velocity whereas increasing carbonisation temperature generally reduces the wear response with in the investigated range. The contour plot highlights the region associated with lower erosive wear, while the three dimensional response surfaces illustrate the magnitude and direction of the response variation. These graphical trends are consistent with regression model and the ANOVA results particularly the significant quadratic effect of carbonisation temperature (CT^2, $p = 0.022$) and the dominant contribution of impact velocity (42.81%).

Surface analysis

Figure 9 represents the SEM of eroded test surfaces at different impact velocities (48 and 72 m/s). As the velocity increases, the eroded surface undergoes plastic deformation, and subsurface cracking is observed due to the impact of particles. Even melting at the impacted surface may happen at high particle velocities. The detachment of filler materials was also observed in higher impact velocities led formation of cavities (Fig. 9a). On the other hand, at low velocity, the stress due to impact is insufficient for plastic deformation, and wear occurs by surface fatigue. Low-impact velocity events can be treated as quasi-static. Impact velocities are classified based on the severity of damage. Low impact velocity is characterized by delamination and matrix cracking, whereas

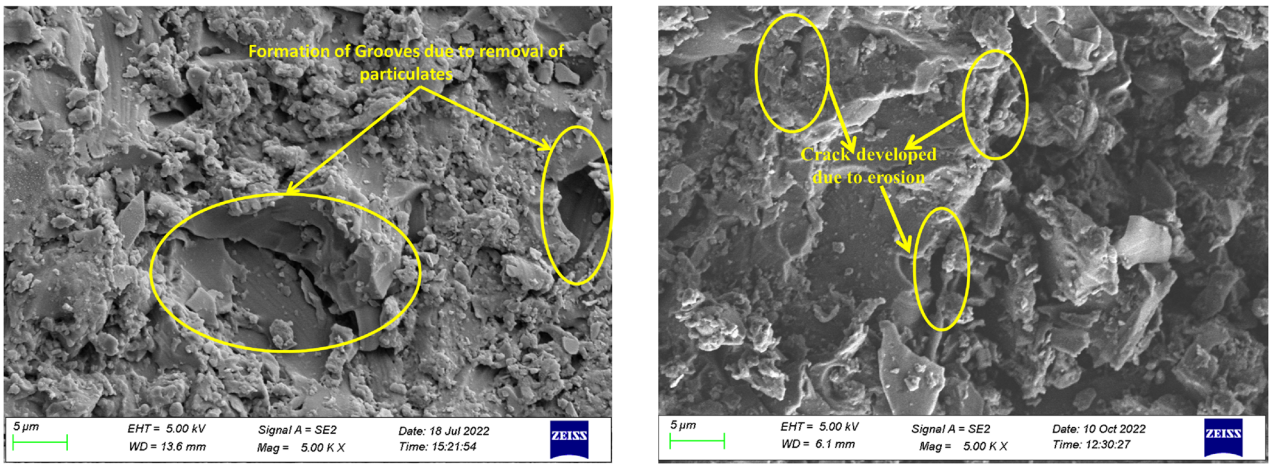

(a) IV - 48 m/s (b) IV - 72 m/s

Fig. 9 SEM micrographs of eroded composite surfaces at different impact velocities: (**a**) 48 m/s and (**b**) 72 m/s.

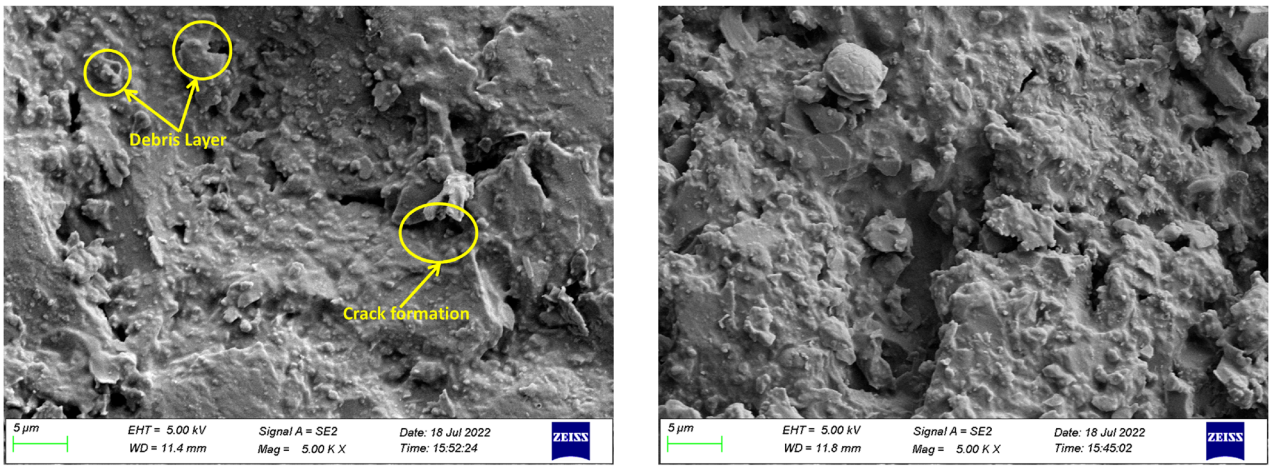

(a) IV - 48 m/s, IA - 45° (b) IV - 72 m/s, IA - 60°

Fig. 10 SEM micrographs of worn surfaces at different IV and IA: (**a**) 48 m/s, 45 and (**b**) 72 m/s, 60 .

high velocity is characterized by penetration that induces debonding and particle pull-out from the surface of the composite material. The material removal rate is at a minimum at low impact velocity. The micro cuts and small craters are clearly visible on the eroded material surface (Fig. 9b).

The worn surfaces of biochar (fabricated at 800 C) reinforced composites under specified operating conditions (48m/s, 45 and 48m/s 60) are shown in Fig. 10a, b. The reduced number of grooves and minor cracks observed after the impact of hard silica particles are consistent with improved interfacial adhesion between the biochar filler and epoxy matrix. As a results voids filler chip out are not seen on the surface of the composite material.

Machine learning analysis

The SVR, RF, and DT ML model prediction performance in estimating the EW output response with IV, CT, IA, and FP input features and comparison with experimental results are discussed in detail in this section. The results discussion is carried out with analysis of ML models metric score calculation from the equations mentioned in Eqs. (3)–(5), and with scattered plot as depicted in Fig. 11. Table. 13 provides the information related to R^2

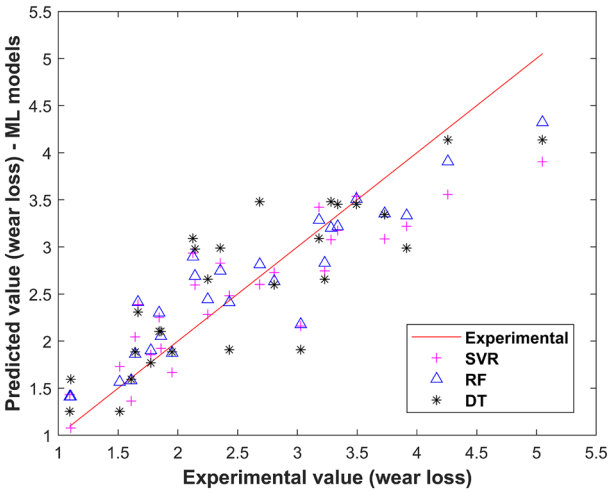

Fig. 11 Comparison of predicted wear loss from ML models with experimental values.

, RMSE, and MAE values for different ML models. The ML models with high R^2 metric score and low RMSE values are considered the best ML models in terms of prediction performance. From Table 13, one can infer that a higher value of R^2 is observed for RF compared to SVR and DT, and low RMSE and MAE values, which demonstrate that RF is the best ML prediction of EW to experimental results, compared to SVR and DT ML models.

The scatter plot of prediction values of EW with different ML models to the EW of experimental results is depicted in Fig. 11. The x-axis and y-axis represent the experimental and ML-predicted EW values. The red line along the diagonal indicates the ideal case where prediction values perfectly match the experimental EW values. The regression plots of SVR, RF, and DT highlight the performance of ML models in predicting EW in comparison to experimental results. From Fig. 11, it is clear that RF shows a close clustering to red line as compared to SVR and DT, which explains the strong alignment between predicted and experimental values. The SVR and DT ML models have a cluster-wise precision that is less than that of RF. This analysis shows that RF outperforms the SVR and DT ML modes in predicting EW values. The experimental and predicted EW values for different ML models are depicted separately in Fig. 12 for better understanding

The optimized parameters for minimizing EW based on the Taguchi optimization method were found to be IV = 48 m/s, CT = 800°C, IA = 60°, and FP = 20 wt.%. The optimized condition was experimentally validated and compared with the ML predictions obtained from the SVR, RF, and DT models. The results are presented separately in Table. 14. The experimental EW was 1.0854, whereas the SVR, RF, and DT models predicted 1.280, 1.130, and 1.208, respectively. Among the three models, RF showed the closest agreement with the experimental result, confirming its superior predictive performance at the optimized condition (Table 12).

To further interpret the Random Forest model, feature importance analysis was performed based on the mean decrease in impurity obtained during tree construction. This analysis quantifies the relative contribution of each machining parameter to the prediction of wear loss. Figure 13 presents the normalized feature importance scores for impact velocity (IV), carbonization temperature (CT), filler percentage (FP), and impact angle (IA). Among the investigated variables, impact velocity exhibited the highest contribution to the predictive capability of the Random Forest model, followed by carbonization temperature and filler percentage, whereas impact angle showed the lowest influence. The obtained ranking is in close agreement with the statistical significance observed from the ANOVA results, thereby providing an independent machine learning-based validation of the dominant process parameters governing erosive wear behavior. The consistency between the statistical and machine learning analyses further enhances the reliability and interpretability of the developed predictive framework.

Although the Random Forest model demonstrated excellent agreement with the experimental measurements, the predictive models remain constrained by the size and range of the available experimental dataset. Consequently, the developed models should be regarded as reliable interpolation tools within the investigated process window rather than universal predictive models for arbitrary processing conditions. Future studies involving

https://doi.org/10.1038/s41598-026-78201-1

Fig. 12 Experimental vs predicted wear loss.

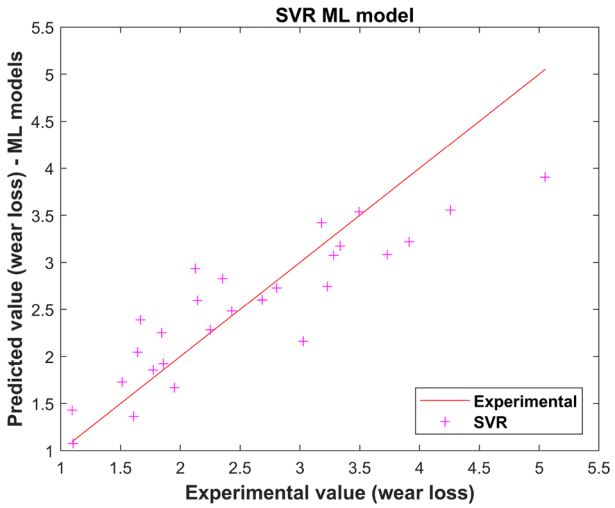

(a) SVR

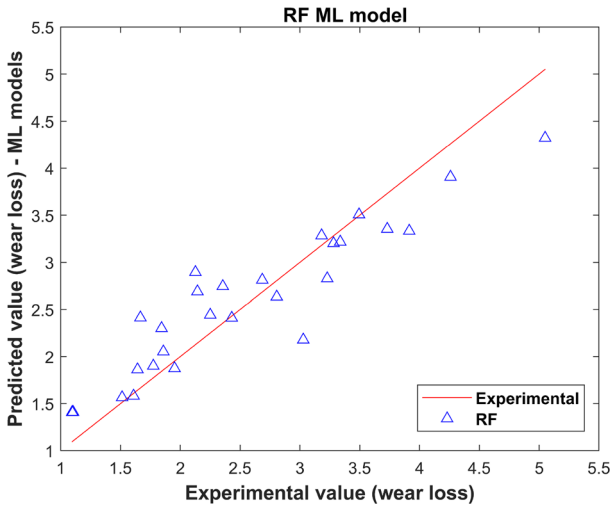

(b) RF

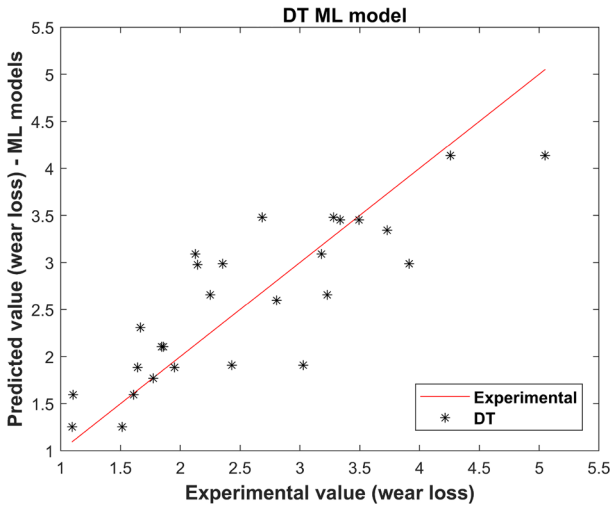

(c) DT

Table 12 Experimental and predicted wear loss using ML models.

Expt.	IV	FP	IA	CT	EW	SVR	RF	DT
1	48	10	45	400	2.43	2.482	2.41	1.906
2	48	15	45	400	3.028	2.161	2.177	1.91
3	48	20	45	400	1.774	1.855	1.9	1.768
4	48	10	60	600	1.642	2.045	1.862	1.884
5	48	15	60	600	1.513	1.729	1.565	1.254
6	48	20	60	600	1.095	1.43	1.408	1.254
7	48	10	90	800	1.952	1.667	1.874	1.884
8	48	15	90	800	1.609	1.363	1.582	1.594
9	48	20	90	800	1.103	1.077	1.41	1.594
10	70	10	60	400	3.181	3.419	3.284	3.089
11	70	15	60	400	3.281	3.07	3.2	3.479
12	70	20	60	400	3.228	2.74	2.828	2.665
13	70	10	90	600	2.126	2.93	2.894	3.089
14	70	15	90	600	2.685	2.6	2.813	3.479
15	70	20	90	600	2.25	2.28	2.442	2.655
16	70	10	45	800	2.143	2.59	2.689	2.976
17	70	15	45	800	1.843	2.25	2.3	2.104
18	70	20	45	800	1.858	1.92	2.05	2.104
19	82	10	90	400	5.05	3.9	4.32	4.136
20	82	15	90	400	4.259	3.55	3.905	4.136
21	82	20	90	400	3.914	3.217	3.33	2.986
22	82	10	45	600	3.494	3.536	3.5	3.452
23	82	15	45	600	3.337	3.175	3.217	3.452
24	82	20	45	600	2.355	2.826	2.745	2.986
25	82	10	60	800	3.73	3.08	3.353	3.3415
26	82	15	60	800	2.806	2.728	2.634	2.597
27	82	20	60	800	1.666	2.387	2.41	2.308

Table 13 Performance metrics of ML models.

Model	R^2	RMSE	MAE
SVR	0.7643	0.4748	0.368
RF	0.8356	0.3965	0.309
DT	0.7064	0.5290	0.416

Table 14 Experimental and ML-predicted EW at the optimized condition.

Parameter combination	Experimental	SVR	RF	DT
IV1FP3CT3IA2	1.0854	1.28	1.13	1.208

larger experimental datasets covering broader operating conditions would further improve model robustness and generalization capability.

Conclusion

In the current research work, CB filler materials derived from OP particulates at different carbonization temperatures were analyzed by FESEM and EDX. Subsequently, biochar is used as a filler in epoxy resin to fabricate composite material. FESEM showed an organized structure for these samples. EDX analysis showed an increase in carbon content in relation to the carbonization temperature. The EW behavior of biochar-reinforced polymer composites was studied successfully in an erosion test rig under different operating conditions using the Taguchi

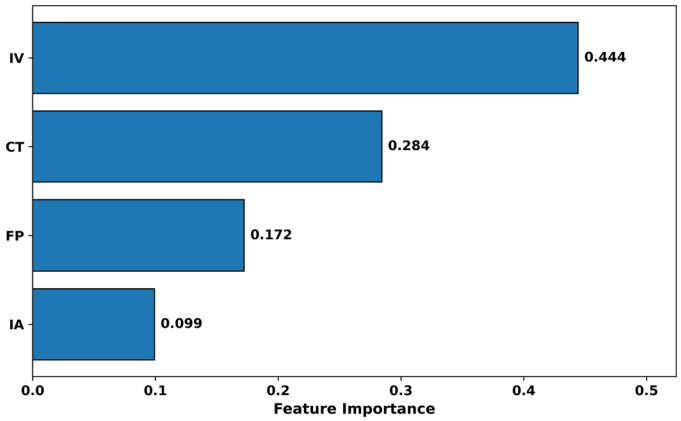

Fig. 13 Feature importance analysis of process parameters in random forest-based wear prediction.

experimental design. The Taguchi approach was utilized to examine the influence of several parameters, including impact velocity, impact angle, carbonization temperature, and filler percentage, on the erosive wear behavior of biochar-reinforced polymer composites. After the test, the results were analyzed, and the conclusions based on the experimental results are presented here as follows.

- Taguchi experimental design is recognized as a simple but effective and systematic approach for assessing the erosion characteristics of biochar-reinforced polymer composites. The composites produced with 20 wt% filler loading and 80 wt% polymer demonstrate superior wear resistance when compared to other specimens. The biochar filler produced at a carbonization temperature of 800 C exhibits the highest wear resistance.
- ANOVA was used to determine the percentage contribution of each factor analyzed. It indicated that impact velocity and carbonization temperature were the most significant factors affecting erosive wear loss, contributing 45.17% and 32.55%, respectively.
- Wear prediction was carried out using a machine learning model, which was then compared to a standard regression method to evaluate performance. The bio-composites reinforced with 20 wt% filler material, manufactured at a carbonization temperature of 800 Celsius, exhibited the lowest wear loss.
- The optimal process parameters for minimizing wear loss were identified as: impact velocity of 48 m/s, impact angle of 60 , filler loading of 20 wt.%, and carbonization temperature of 800 C.
- Carbonization enhances the physicochemical properties of the filler material by increasing its surface area and adsorption capacity, thereby improving interfacial bonding between filler and matrix.
- Biochar composites prepared at a higher carbonization temperature (800 C) exhibited superior erosion resistance compared to other combinations investigated in this study.
- Machine learning models proved to be effective tools for predicting EW. Among the models considered, the Random Forest model demonstrated superior performance compared to support vector regression and decision tree models.
- This research work opens up a new opportunity for a value-added utilization of a biowaste material in designing and manufacturing erosion-resistant polymer composites. These composites are used in tribological applications such as doors and window panels, floor tiles, etc., where erosive wear is the main criterion of failure.

The developed composites demonstrate potential for erosion wear applications such as slurry pipelines, cyclone separators, ducting systems, fan blades, and material handling equipment. Their improved erosion resistance can enhance component durability and reduce maintenance costs. Nevertheless, performance may be influenced by service conditions, including particle velocity, impact angle, temperature, and environmental exposure. Further studies involving long-term field conditions and combined wear mechanisms are required to fully establish the suitability of these composites for industrial deployment.

Author contributions P.N.: Conceptualization; methodology; experimentation; software; validation; formal analysis; In-

vestigation; data curation; Writing—original draft; writing—review and editing; visualization. T.R.K.: Conceptualization; methodology; software; validation; formal analysis; writing—original draft; writing—review and editing; visualization. S.P.: Conceptualization; methodology; experimentation; software; validation; formal analysis; investigation; data curation; writing—original draft; writing—review and editing. B.K.: Validation; software; methodology; investigation; formal analysis. Z.N.N.: Validation; software; methodology; formal analysis; writing—review and editing. All authors read and approved the final manuscript.

Funding The author did not receive funding from any organization for the conduct of this work.

Data availability The data required to produce the results are presented in the paper.

Declarations

Competing interests The authors declare no competing interests.

Declaration of generative AI and AI-assisted technologies in the manuscript preparation process. During the preparation of this work, the author(s) used ChatGPT in order to improve the academic language, clarity, coherence, and structural organization of the manuscript. After using this tool, the author(s) carefully reviewed and edited the content as needed and take(s) full responsibility for the integrity and scientific content of the published article.

Open Access This article is licensed under a Creative Commons Attribution 4.0 International License, which permits use, sharing, adaptation, distribution and reproduction in any medium or format, as long as you give appropriate credit to the original author(s) and the source, provide a link to the Creative Commons licence, and indicate if changes were made. The images or other third party material in this article are included in the article's Creative Commons licence, unless indicated otherwise in a credit line to the material. If material is not included in the article's Creative Commons licence and your intended use is not permitted by statutory regulation or exceeds the permitted use, you will need to obtain permission directly from the copyright holder. To view a copy of this licence, visit http://creativecommons.org/licenses/by/4.0/.

References

1. Karataş, M. A. & Gökkaya, H. A review on machinability of carbon fiber reinforced polymer (CFRP) and glass fiber reinforced polymer (GFRP) composite materials. *Defence Technol.* **14**, 318–326. https://doi.org/10.1016/j.dt.2018.02.001 (2018).
2. Rajak, D. K., Wagh, P. H. & Linul, E. Manufacturing technologies of carbon/glass fiber-reinforced polymer composites and their properties: a review. *Polymers* **13**, 3721. https://doi.org/10.3390/polym13213721 (2021).
3. Kumar, M., Jena, H. & Pradhan, P. Impact of filler on solid particle erosion wear in glass fibre composites: a comprehensive review. *Proc. IMechE Part E J. Process Mech. Eng.* https://doi.org/10.1177/09544089251326998 (2024).
4. Verma, S. K., Gangil, B., Gupta, A., Rajput, N. S. & Singh, T. Dolomite dust filled glass fiber reinforced epoxy composite: influence of fabrication techniques on physicomechanical and erosion wear properties. *Polym. Compos.* **43**, 551–565. https://doi.org/10.1002/pc.26398 (2022).
5. Sharma, H. B. et al. Circular economy approach in solid waste management system to achieve UN-SDGs: Solutions for post-COVID recovery. *Sci. Total Environ.* **800**, 149605. https://doi.org/10.1016/j.scitotenv.2021.149605 (2021).
6. Sangilimuthukumar, J. et al. Erosion characteristics of epoxy-based jute, kenaf and banana fibre reinforced hybrid composites. *Mater. Today: Proc.* **64**, 6–10. https://doi.org/10.1016/j.matpr.2022.03.469 (2022).
7. Purohit, A., Dehury, J., Rout, L. N. & Pal, S. A novel study of synthesis, characterization and erosion wear analysis of glass-jute polyester hybrid composite. *J. Inst. Eng. India Ser. E* **104**, 1–9. https://doi.org/10.1007/s40034-023-00268-6 (2023).
8. Sahu, P. & Gupta, M. K. Enhancement in erosion wear resistance of sisal composites by eco-friendly treatment and coating. *Mater. Res. Express* **6**, 085348. https://doi.org/10.1088/2053-1591/ab29b5 (2019).
9. Sundarakannan, R. et al. Importance of fiber-/nanofiller-based polymer composites in mechanical and erosion performance: A review. *J. Nanomater.* **1–16**, 2023. https://doi.org/10.1155/2023/3528977 (2023).
10. Sivasaravanan, S., Sangeetha, M., Prakash, S., Reddy, T. D. & Rahul, D. P. Experimental investigation of composite material laminated with aloe vera fiber in different composite resin. *Mater. Today: Proc.* **16**, 832–837. https://doi.org/10.1016/j.matpr.2019.05.165 (2019).

11. Sharma, A., Choudhary, M., Agarwal, P., Biswas, S. K. & Patnaik, A. Review on erosion wear characteristic of natural fiber reinforced polymer composite. *Mater. Today Proc.* **44**, 4795–4800. https://doi.org/10.1016/j.matpr.2020.11.395 (2021).
12. Patnaik, A., Satapathy, A., Chand, N., Barkoula, N. M. & Biswas, S. Solid particle erosion wear characteristics of fiber and particulate filled polymer composites: a review. *Wear* **268**, 249–263 (2010).
13. Rajendran, S. et al. Solid particle erosion in fibre composites: a review. *J. Reinf. Plast. Compos.* https://doi.org/10.1177/07316844241255007 (2024).
14. Liu, W. J., Jiang, H. & Yu, H. Q. Development of biochar based functional materials: toward a sustainable platform carbon material. *Chem. Rev.* **115**, 12251–12285. https://doi.org/10.1021/acs.chemrev.5b00195 (2015).
15. Infurna, G., Caruso, G. & Dintcheva, N. T. Sustainable materials containing biochar particles: a review. *Polymers* **15**, 343. https://doi.org/10.3390/polym15020343 (2023).
16. Bartoli, M., Arrigo, R., Malucelli, G., Tagliaferro, A. & Duraccio, D. Recent advances in biochar polymer composites. *Polymers* **14**, 2506. https://doi.org/10.3390/polym14122506 (2022).
17. Aboughaly, M., Babaei-Ghazvini, A., Dhar, P., Patel, R. & Acharya, B. Enhancing the potential of polymer composites using biochar as a filler: a review. *Polymers* **15**, 3981. https://doi.org/10.3390/polym15193981 (2023).
18. Mamand, D. M. et al. Enhanced optical properties of chitosan polymer doped with orange peel dye investigated via UV-Vis and FTIR analysis. *Sci. Rep.* **15**, 3232. https://doi.org/10.1038/s41598-025-87425-6 (2025).
19. Hristea, G., Iordoc, M., Lungulescu, E.-M., Bejenari, I. & Volf, I. A sustainable bio-based char as emerging electrode material for energy storage applications. *Sci. Rep.* **14**, 1095. https://doi.org/10.1038/s41598-024-51350-x (2024).
20. Gunasekaran, Y. et al. Synthesis and characterization of ZnO/biochar composite as electrode material for hybrid supercapacitor. *Ionics* **32**, 1987–2010. https://doi.org/10.1007/s11581-025-06839-4 (2026).
21. Koppiahraj, K., Bathrinath, S., Narayanasamy, P. et al. A review on the factors influencing natural fiber composite materials. In: *Hybrid Natural Fiber Composites*, 185–205. https://doi.org/10.1016/B978-0-12-819900-8.00003-9 (Elsevier, 2021).
22. Sahu, P. & Gupta, M. K. A review on the properties of natural fibres and its bio-composites: effect of alkali treatment. *Proc. Inst. Mech. Eng. Part L J. Mater. Design Appl.* **234**, 198–217. https://doi.org/10.1177/1464420719888820 (2020).
23. Hasan, K. F., Horváth, P. G. & Alpár, T. Potential natural fiber polymeric nano biocomposites: a review. *Polymers* **12**, 1072. https://doi.org/10.3390/polym12051072 (2020).
24. Richard, S., Selwin Rajadurai, J. & Manikandan, V. Effects of particle loading and particle size on tribological properties of biochar particulate reinforced polymer composites. *J. Tribol.* **139**, 012202. https://doi.org/10.1115/1.4033131 (2017).
25. Prasad, B. S. & Balaji, A. Study on engineering properties of bamboo fiber/biochar reinforced epoxy composites rod. *Biomass Convers. Biorefinery* **15**, 1525–1534. https://doi.org/10.1007/s13399-024-05754-4 (2025).
26. Chueangchayaphan, N., Tarasin, M., Phonjon, W. & Chueangchayaphan, W. Evaluating oil palm trunk biochar and palm oil as environmentally friendly sustainable additives in green natural rubber composites. *Polymers* **17**, 223. https://doi.org/10.3390/polym17020223 (2025).
27. Girish, G. B., Veeresh, H. & Ramesh, B. T. Effect of pistachio nano-particles on wear properties of wood apple and coconut shell powder reinforced hybrid composites. *J. Inst. Eng. (India) Ser. C* **104**, 979–988. https://doi.org/10.1007/s40032-023-00879-3 (2023).
28. Zainal Abidin, Z., Mamauod, S. N. L., Romli, A. Z., Sarkawi, S. S. & Zainal, N. H. Synergistic effect of partial replacement of carbon black by palm kernel shell biochar in carboxylated nitrile butadiene rubber composites. *Polymers* **15**, 943. https://doi.org/10.3390/polym15040943 (2023).
29. Sutikno, M., Marwoto, P. & Rustad, S. The mechanical properties of carbonized coconut char powder-based friction materials. *Carbon* **48**, 3616–3620. https://doi.org/10.1016/j.carbon.2010.06.015 (2010).
30. Ojha, S., Acharya, S. K. & Raghavendra, G. Mechanical properties of natural carbon black reinforced polymer composites. *J. Appl. Polym. Sci.* https://doi.org/10.1002/app.41211 (2015).
31. Samantrai, S. P., Raghavendra, G. & Acharya, S. K. Effect of carbonization temperature and fibre content on the abrasive wear of rice husk char reinforced epoxy composite. *Proc. IMechE Part J.* **228**, 463–469. https://doi.org/10.1177/1350650113516435 (2014).
32. Betancourt, S., Cruz, L. J. & Toro, A. Effect of the addition of carbonaceous fibers on the tribological behavior of a phenolic resin sliding against cast iron. *Wear* **272**, 43–49 (2011).
33. Giorcelli, M., Savi, P., Khan, A. & Tagliaferro, A. Analysis of biochar with different pyrolysis temperatures used as filler in epoxy resin composites. *Biomass Bioenerg.* **122**, 466–471. https://doi.org/10.1016/j.biombioe.2019.01.007 (2019).
34. Minugu, O. P. et al. Effect of biomass-biochar content on the erosion wear performance of biochar epoxy composites. *Polym. Compos.* **43**, 3189–3203. https://doi.org/10.1002/pc.26610 (2022).
35. Johnson, R., Arumugaprabu, V., Kumar, M. P. & Dheeraj, K. Solid particle erosion on the biochar filled hybrid vinyl ester composite. In: *AIP Conference Proceedings*, vol. 2057. https://doi.org/10.1063/1.5085635 (2019).
36. Sundarakannan, R. et al. Effect of polyethylene terephthalate char on impact and erosion properties of polyester matrix composites. *Adv. Mater. Process. Technol.* **8**, 4122–4135. https://doi.org/10.1080/2374068X.2022.2036589 (2022).

37. Li, W. et al. Effects of carbonization temperatures on characteristics of porosity in coconut shell chars. *Ind. Crops Prod.* **28**, 190–198. https://doi.org/10.1016/j.indcrop.2008.02.012 (2008).
38. Panchal, M., Minugu, O. P., Gujjala, R. & Ojha, S. Study of environmental behavior and its effect on solid particle erosion behavior of hierarchical porous activated carbon-epoxy composite. *Polym. Compos.* **43**, 2276–2287. https://doi.org/10.1002/pc.26539 (2022).
39. Prakash, M. O., Raghavendra, G. & Ojha, S. Investigation of tribological properties of biomass developed porous nano activated carbon composites. *Wear* **466**, 203523. https://doi.org/10.1016/j.wear.2020.203523 (2021).
40. Łożyńska, M. et al. The application of biochar as an alternative to graphite in mineral greases-tribological and rheological property studies. *Ind. Crops Prod.* **242**, 122913. https://doi.org/10.1016/j.indcrop.2026.122913 (2026).
41. Yadav, A. K. & Mishra, S. Fabrication and characterization of mechanical properties of stacked hybrid composites reinforced with natural fibers and groundnut shell powder as biochar. *Polym. Renew. Resour.* https://doi.org/10.1177/20412479261461266 (2026).
42. Kozdrach, R. & Radulski, P. Influence of a walnut shell biochar additive on the tribological and rheological properties of vegetable lubricating grease. *Lubricants* **13**, 213. https://doi.org/10.3390/lubricants13050213 (2025).
43. Supriya, J., Shetty, R., Naik, N., Maddasani, S. & Hegde, A. Chemical characterization of hibiscus rosa-sinensis plant fibers facilitated through design of experiments and artificial neural network hybrid approach. *Sci. Rep.* **14**, 22510. https://doi.org/10.1038/s41598-024-73503-8 (2024).
44. Naik, P., Pradhan, S., Acharya, S. K. & Sahoo, P. Effect of carbonization of orange peel particulate-reinforced polymer composites. *IJSEIMS* **10**, 1–20. https://doi.org/10.4018/IJSEIMS.295097 (2022).
45. Naik, P., Acharya, S. K., Sahoo, P. & Pradhan, S. Abrasive wear behaviour of orange peel particulate reinforced polymer composites. *Proc. IMechE Part J.* **235**, 2099–2109. https://doi.org/10.1177/1350650121991412 (2021).
46. Naik, P., Sahoo, P., Acharya, S. K. & Pradhan, S. Erosive wear behaviour of bio-waste particulate-reinforced epoxy composites. *J. Indian Acad. Wood Sci.* **18**, 1–3. https://doi.org/10.1007/s13196-020-00272-y (2021).
47. Awad, H. H. & Desouki, M. Multifunctional performance assessment of waste-based bioplastic wall panels for acoustic thermal and structural efficiency in interior architecture. *Sci. Rep.* **15**, 15708. https://doi.org/10.1038/s41598-025-98326-z (2025).
48. Menda, V. R. et al. Machine learning based prediction of the performance and emission characteristics of CRDI diesel engine using diethyl ether and carbon nanotube additives with spirulina platensis as a third-generation biofuel. *Sci. Rep.* **15**, 39958. https://doi.org/10.1038/s41598-025-23747-9 (2025).
49. Kumar, T. R. Numerical simulation and machine learning framework approach for ballistic performance evaluation of aluminium structures. *Res. Eng.* https://doi.org/10.1016/j.rineng.2025.108788 (2025).
50. Bikkavolu, J. R. et al. Predicting common rail direct injection (CRDI) engine metrics using nanoparticle-enhanced *Pongamia pinnata* biodiesel with machine learning. *Emergent Mater.* https://doi.org/10.1007/s42247-025-01175-9 (2025).
51. Tota, R. K., Nagaraju, D., Syed, J. & Mohammad, A. R. Performance of heat transfer in AL2o3/MWCNT hybrid nanofluid flow using machine learning models. *Eng. Res. Express* **7**, 015528. https://doi.org/10.1088/2631-8695/adaadb (2025).
52. Cui, Y. et al. Sustainable performance enhancement of a heat recovery ground source heat pump system using field data and machine learning. *Sci. Rep.* https://doi.org/10.1038/s41598-026-45353-z (2026).
53. Harishbabu, S. et al. Machine learning and response surface methodology for optimization and prediction of tribological performance of pla/rice husk biochar composites. *Sci. Rep.* https://doi.org/10.1038/s41598-026-51463-5 (2026).
54. Vapnik, V. N. *The Nature of Statistical Learning Theory* (Springer, 1995).
55. Breiman, L. Random forests. *Mach. Learn.* **45**, 5–32. https://doi.org/10.1023/A:1010933404324 (2001).
56. Hornik, K., Stinchcombe, M. & White, H. Multilayer feedforward networks are universal approximators. *Neural Netw.* **2**, 359–366. https://doi.org/10.1016/0893-6080(89)90020-8 (1989).
57. Chen, J. et al. A complete review on the oxygen-containing functional groups of biochar: formation mechanisms, detection methods, engineering, and applications. *Sci. Total Environ.* **946**, 174081. https://doi.org/10.1016/j.scitotenv.2024.174081 (2024).
58. Loc, N. X. & Do, T. M. Optimizing biochar production: a review of recent progress in lignocellulosic biomass pyrolysis. *Eng. Agric.* **12**, 148. https://doi.org/10.15302/J-FASE-2024597 (2025).
59. Abbas, A., Afzal, S., Waseem, M., Ahmad, M. & Xu, D. Advances in biochar production and performance for sustainable environment and energy applications. *Sustainability* **18**, 5865. https://doi.org/10.3390/su18125865 (2026).
60. Shunmugesh, K. et al. Enhancing drilling performance in 3D printed PLA implants application of PIV and ML models. *Sci. Rep.* **15**, 13314. https://doi.org/10.1038/s41598-025-96126-z (2025).
61. Shaik, A. S. et al. Machine learning prediction and hybrid GRA-AHP optimization of AWJM parameters of ultrasonic assisted stir cast AL6061-B_4C-ZRo_2 composites. *Sci. Rep.* https://doi.org/10.1038/s41598-026-58314-3 (2026).
62. Selvan, D. K. et al. Investigation of tribological behaviour of b4C-graphene glass fiber composites using Taguchi, multi-criteria decision making, and machine learning approaches. *J. Compos. Mater.* https://doi.org/10.1177/00219983261450597 (2026).

Publisher's note Springer Nature remains neutral with regard to jurisdictional claims in published maps and institutional affiliations.

Authors and Affiliations

Smitirupa Pradhan[1] · Prajapati Naik[2] · Rakesh Kumar Tota[3] · Kamesh Bodduru[4] · Nankwaya Ntumba Zacharie[5]

✉ Prajapati Naik
prajapati.naik@nist.edu

✉ Nankwaya Ntumba Zacharie
zacharientumba10@gmail.com

1 School of Mechanical Engineering, KIIT University, Bhubaneswar, Odisha 751024, India

2 Department of Mechanical Engineering, NIST University, Institute Park, Berhampur, Odisha 761008, India

3 School of Marine Engineering and Technology, Indian Maritime University, Chennai, Tamil Nadu 600119, India

4 Department of Mechanical Engineering, Sharda University, Greater Noida 201310, India

5 Kinshasa, Ngaliema, Democratic Republic of Congo